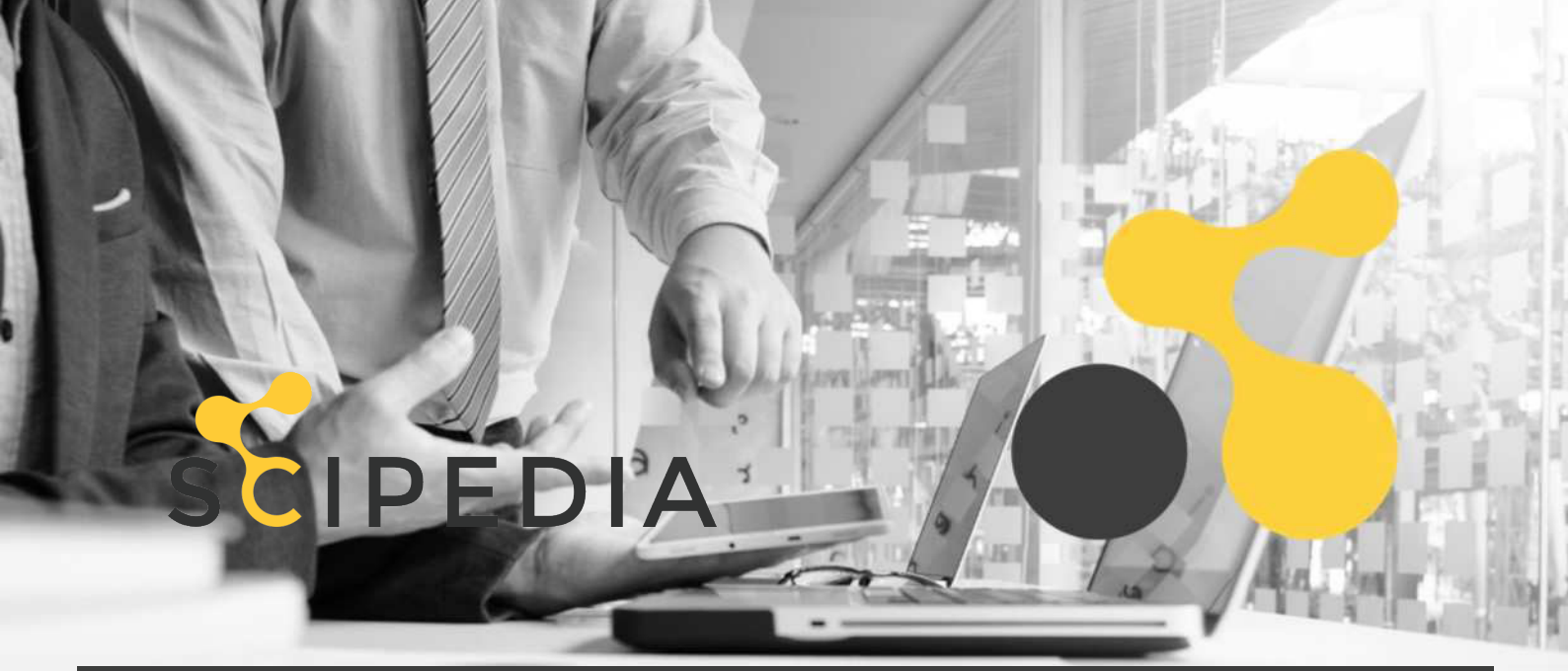

# Proposal and Energy Analysis of a New Design Integrating the SCPP into Electricity Pylon Using CFD Numerical Method: Towards Ensuring Electric Needs of Rural Dwellings

Ammar Mebarki[1,*] and Meriem Hafidha Titi[2]

[1] Institute of Architecture and Urbanism, University of Batna 1, Batna, 05000, Algeria

[2] Laboratory of Architecture, Urbanism, and Transport: Habitat, landscape and urban mobility (LAUTr), Institute of Architecture and Urbanism, University of Batna 1, Batna, 05000, Algeria


**INFORMATION**

**Keywords:**
Pylons
SCPP
turbine position
collector radius
CFD
rural dwellings
electricity

**DOI:** 10.23967/j.rimni.2025.10.74691

SCIPEDIA Revista Internacional de Métodos Numéricos para Cálculo y Diseño en Ingeniería

Revista Internacional Métodos numéricos para cálculo y diseño en ingeniería RIMNI

In cooperation with CIMNE

# Proposal and Energy Analysis of a New Design Integrating the SCPP into Electricity Pylon Using CFD Numerical Method: Towards Ensuring Electric Needs of Rural Dwellings

**Ammar Mebarki**[1,*] **and Meriem Hafidha Titi**[2]

[1]Institute of Architecture and Urbanism, University of Batna 1, Batna, 05000, Algeria

[2]Laboratory of Architecture, Urbanism, and Transport: Habitat, landscape and urban mobility (LAUTr), Institute of Architecture and Urbanism, University of Batna 1, Batna, 05000, Algeria

## ABSTRACT

Rural electrification is critical for increasing agricultural output, thereby reducing poverty and improving food security. Electricity pylons are steel structures that transport electricity at high voltages and are often the tallest objects in the countryside. The current study proposes a novel solar chimney power plant (SCPP) model in which the chimney is contained within the pylon's vertical structure. The numerical methodology was carried out using Manzanares' SCPP 3D axisymmetric CFD model, which was simulated with ANSYS Fluent software. The RNG k-$\varepsilon$ turbulence model and a discrete ordinates non-grey radiation model were used. Following model validation, the results led to the identification of five turbine positions based on five collector radius intervals. To the best of our knowledge, this is the first time this has been observed in the SCPP system as a result of air velocity variations throughout the chimney. Equations based on collector radius and solar radiation are used to calculate the generated electric energy and the number of rural houses that could be electrified at each interval. Our findings confirmed the proposed model's efficiency in generating electricity; for instance, one hour of 1000 W/m$^2$ solar radiation using a collector radius of 200 m produces 14.82 kW that could supply 6.877 rural houses in India or 7.411 rural houses in China for 24 h. This study proposes a plan for electricity transmission companies to invest in infrastructure (pylons) to provide rural renewable electricity.

**OPEN ACCESS**

**Received:** 16/10/2025

**Accepted:** 27/11/2025

**DOI**
10.23967/j.rimni.2025.10.74691

**Keywords:**
Pylons
SCPP
turbine position
collector radius
CFD
rural dwellings
electricity

## Nomenclatures

| | |
|---|---|
| $Cp$ | Specific heat capacity of the air (J kg$^{-1}$ K$^{-1}$) |
| $r$ | Collector radius (m) |
| $Ri$ | Richardson number |
| $g$ | Gravitational acceleration (m s$^{-2}$) |
| $Hch$ | Chimney height (m) |
| $G$ | Global radiation (W m$^{-2}$) |
| $k$ | Turbulent kinetic energy (m$^2$ s$^{-2}$) |

*Correspondence: Ammar Mebarki (ammar.mebarki@univ-batna.dz). 

| | |
|---|---|
| $\Delta p$ | Pressure (Pa) |
| $P$ | Electric power (KW) |
| $Pr$ | Prandtl number |
| $T$ | Temperature (K) |
| $V$ | Air velocity (m $s^{-1}$) |
| $b$ | Thermal expansion coefficient |
| $\varepsilon$ | Dissipation rate of turbulent kinetic energy ($m^2$ $s^{-3}$) |
| $m$ | Dynamic viscosity ($m^2$ $s^{-1}$) |
| $r$ | Air Density (kg $m^{-3}$) |

## 1 Introduction

With the introduction of new technologies, such as heat pumps and electric vehicles, electrical consumption has skyrocketed. Buildings account for 40% of global energy consumption and 25% of net greenhouse gas emissions [1,2]. Furthermore, the war in Ukraine has resulted in a fuel energy crisis, raising the global cost of electricity generation. Indeed, despite pressure from many governments to reduce electric consumption, it increased to 2% by the end of 2022 [3], emphasizing the importance of finding efficient solutions for using renewable alternative energy.

The majority of rural residents rely on agriculture as their primary source of income. Similarly, rural electrification aims to increase agricultural output in order to reduce poverty and improve food security [4]. Many researchers investigated the issue of power supply in rural areas, taking into account the high economic costs of connecting to energy supply networks. Uski et al. (2018) conducted a sensitivity analysis of microgrid investment options to ensure power supply reliability in rural networks as an alternative to underground cabling [5]. Moreover, Gunasekaran (2020) looked into the concept of a manufacturing incubator to assist rural electric cooperatives in becoming self-sufficient in terms of electrical system needs through local manufacturing [6].

Off-grid solar photovoltaic energy offers a viable alternative to centrally distributed electricity in developing countries [7]. These off-grid energy systems operate without the extensive support networks associated with centralized power generation, allowing rural areas to overcome critical barriers in the energy transition process [8]. Urpelainen et al. (2016) demonstrated that microgrids are becoming more widely recognized as a viable alternative to traditional grid infrastructure for connecting underserved populations and ensuring a sustainable energy supply [9,10].

Several studies in the literature have emphasized the ability of stand-alone renewable off-grid systems in developing countries to promote economic development while also ensuring environmental sustainability [11,12]. For example, previous research in India has shown that providing solar power locally in villages can overcome the political challenges that Indian energy sector reforms typically face [13].

The solar chimney power plant (SCPP) is a renewable-energy system that generates electricity. It has recently gained popularity due to its ability to generate green energy. This system consists of three main components: a long cylindrical structure typically located in the center of a greenhouse collector made of transparent plastic films or glass, and a turbine placed at the base or inside the chimney [14]. The SCPP operates by converting solar energy into thermal energy within a collector. This thermal energy is then transformed into kinetic energy as heated air rises through a chimney, ultimately generating electricity via a wind turbine coupled with a generator. This system is clean, simple, durable, and capable of producing large-scale renewable electricity with very low operating costs and extended daily generation [14].

Although the concept of the solar chimney was introduced in 1903, its first successful implementation occurred in the 1980s in Manzanares, Spain, through the efforts of Caicedo et al. and Schlaich et al. The SCPP analyzed in the study features a chimney measuring 194.6 m in height and 5.08 m in radius, while the collector is positioned 1.85 m above the ground with a radius of 122 m [15–18].

The collector enables solar radiation to penetrate the air volume between it and a 6000 $m^2$ soil surface. The greenhouse effect driven by the soil's absorptivity results in the absorption of solar radiation, which heats the soil and consequently the overlying air. As the air temperature increases, its density decreases, causing it to rise and accelerate due to the pressure differential created by the tall chimney. Although the primary energy source for the system is daily solar radiation, the pressure gradient between the chimney's inlet and outlet allows the system to continue operating during nighttime or low-sunlight conditions.

Recent studies have employed numerical simulations to enhance SCPP performance, particularly examining the influence of ground thermal inertia [19]. Additional research has focused on the effects of chimney geometry (including divergence angle), ambient temperature, solar flux and turbine efficiency [20], and chimney height [21]. Solar chimneys have been evaluated across diverse climatic conditions, as reported by Schlaich and Titi et al. [22,23]. While most investigations treat the SCPP as a standalone system, some have explored its integration with existing structures. For instance, Wang et al. [24], proposed the coupling of solar chimneys with buildings and telecommunications towers, highlighting their potential as multifunctional infrastructure elements.

Electricity pylons, also known as transmission towers, are tall steel structures used to transport high-voltage electricity. The word pylon is derived from the Greek word '*pyle*', meaning 'gateway'. During the 1920s, the first steel pylons were built, becoming the gateways to electricity for everyone [25]. These pylons are usually the tallest structures in the countryside [26]. The height of pylons varies depending on factors such as the ground height from which they rise and the distance between them [27]. Tall pylons allow the wires to cross rivers, railways, and roads. For example, the National Grid pylons in the United Kingdom are at least 36 m tall [25]. Given that these large structures are indispensable and widely distributed around the world, it appears critical to find an environmental use for them, such as producing renewable energy, as proposed by Perales et al. (2019). The researchers of the previously mentioned study concentrated on the arrangement of cross-flow turbine blades and the development of an electric generation system intended for rural homes [28].

This study is based on selecting and implementing a model from one of the most well-known and widely distributed electricity pylons for the production of clean electricity via the solar chimney power plant (SCPP) system. The integration of an SCPP with existing transmission pylons aims to reuse land and structures already available in power corridors, avoiding the need to build a separate tall chimney. This approach reduces environmental and structural costs while enabling small, distributed renewable generation directly on the grid.

## 2 Materials and Methods

### *2.1 The Novel SCPP Proposed Model*

The tower model announced in the Central Electricity Board's annual report for 1927 in the United Kingdom was chosen as the basis for the proposed shape and dimensions of the solar chimney power plant, which is considered one of the most widely used types of pylons worldwide [25]. This paper proposes a new design for solar chimneys that corresponds to the shape of the chosen pylon, tests the effect of collector diameters on system outputs, and investigates the best height for placing the

turbine. We integrated the solar chimney into the pylon, resulting in a vertical structure that houses the Polyvinyl Chloride (PVC) chimney. The collector is made of transparent plastic films that are designed to look like the original model from Manzanares, Spain.

Given that the distance between pylons is typically limited to 200 m, the collectors tested in this study have diameters of 40, 80, 120, 160, and 200 m. In order to reconcile the usual spacing of the pylons (≈200 m), the practical implementation proposed in the study is based on an alternating strategy: only the alternating pylons (e.g., one pylon out of three or more) are equipped with a collector and an integrated chimney; the intermediate pylons remain unequipped.

The collector was exposed to various solar radiation levels (1000, 800, 600, and 400 W/m$^2$). Fig. 1 illustrates the details and dimensions of the proposed model. In this system, solar energy is converted into thermal energy in the collector, then to kinetic energy in the chimney, and finally to electrical energy via a generator and a wind turbine [14,29].

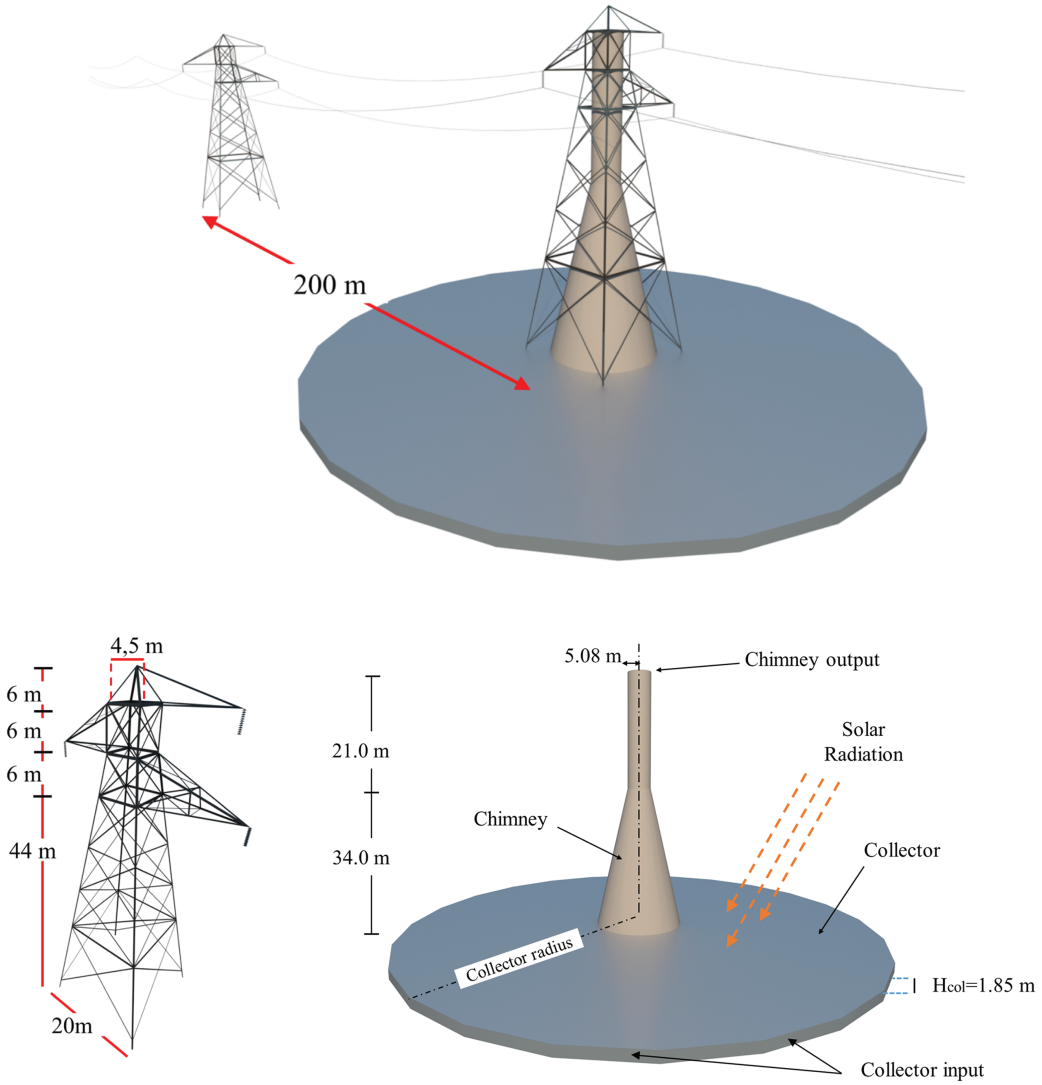


**Figure 1:** The proposed model: solar chimney power plant integrated with the chosen pylon

### *2.2 The Numerical Model*

While some research on SCPP focuses on numerical model optimization [30,31], the majority of SCPP studies use CFD techniques. Elwekeel et al. (2018) used the ANSYS Fluent solver to analyze the effect of numerical model parameters on the accuracy of computational outcomes. They discovered that the ek-$\varepsilon$ model is the most effective model to predict the SCPP characteristics, based on their investigation of the effect of the turbulence model on air flow within SCPP [32]. The governing equations for continuity, momentum, and energy transport describe the interior flow of a solar chimney [33,34]:

$$\frac{\partial \rho}{\partial t} + \frac{1}{r}\frac{\partial (\rho u r)}{\partial r} + \frac{\partial (vr)}{\partial z} = 0 \tag{1}$$

$$\frac{\partial (pu)}{\partial t} + \frac{1}{r}\frac{\partial}{\partial r}(pruu) + \frac{\partial (\rho uv)}{\partial z} = -\frac{\partial p}{\partial r} + \frac{1}{r}\frac{\partial}{\partial r}\left(\mu r \frac{\partial u}{\partial r}\right) + \frac{\partial}{\partial z}\left(\mu \frac{\partial u}{\partial z}\right) - 2\mu \frac{u}{r^2} \tag{2}$$

$$\frac{\partial (\rho v)}{\partial t} + \frac{1}{r}\frac{\partial}{\partial r}(\rho ruv) + \frac{\partial (\rho \vartheta v)}{\partial z} = -\frac{\partial \rho}{\partial z} + \frac{1}{r}\frac{\partial}{\partial r}\left(\mu r \frac{\partial \vartheta}{\partial r}\right) + \frac{\partial}{\partial z}\left(\mu \frac{\partial \vartheta}{\partial z}\right) - (\rho_0 - \rho)\, g \tag{3}$$

Energy equation:

$$\frac{\partial (\rho C_p T)}{\partial t} + \frac{1}{r}\frac{\partial}{\partial r}\left(\rho r C_p u T\right) + \frac{\partial (\rho C_p v T)}{\partial z} = \frac{1}{r}\frac{\partial}{\partial r}\left(r\lambda \frac{\partial T}{\partial r}\right) + \frac{\partial}{\partial z}\left(\lambda \frac{\partial T}{\partial z}\right) - \nabla . q_r \tag{4}$$

The Rayleigh number (Ra) quantifies the strength of buoyancy-induced flow in natural convection:

$$R_a = \frac{g\beta \Delta T L^3}{av} \tag{5}$$

where, $\Delta T$ represents the maximum temperature difference within the system, $\beta$ denotes the thermal expansion coefficient, $L$ signifies the mean height of the collector, and a indicates the thermal diffusivity.

Overall, the analysis of the collector and chimney shows that the Ra value is greater than 1010; thus, fluid flow in the regions may be turbulent [35,36]. The turbulent flow was simulated with the RNG k-model [37]. The turbulence kinetic energy (K) and rate of dissipation can be calculated from the two transport equations as follows [38]:

$$\frac{\partial (\rho k)}{\partial t} + \frac{\partial}{\partial X_i}(\rho K u_i) = \frac{\partial}{\partial X_j}\left(\alpha_k \mu_{eff} \frac{\partial K}{\partial X_j}\right) + G_K + G_b - \rho\varepsilon - Y_M \tag{6}$$

$$\frac{\partial (\rho \varepsilon)}{\partial t} + \frac{\partial}{\partial X_j}(\rho \varepsilon u_i) = \frac{\partial}{\partial X_j}\left(\alpha_\varepsilon \mu_{eff} \frac{\partial \varepsilon}{\partial X_j}\right) + G_{1\varepsilon}\frac{\varepsilon}{k}(G_k + G_{3\varepsilon} G_b) - G_{2\varepsilon}\rho \frac{\varepsilon^2}{k} - R_\varepsilon \tag{7}$$

In this context, $G_k$ represents the generation of turbulent kinetic energy due to mean velocity gradients, while $G_b$ denotes the generation of turbulent kinetic energy attributed to buoyancy. The turbulent Prandtl numbers are defined as $\partial_T = 0.9$, $\partial_k = 1.0$, and $\partial_\varepsilon = 1.3$ for $T$, $k$, and $\varepsilon$, respectively. Additionally, the constants for the turbulent model are $C_{1\varepsilon} = 1.44$, $C_{2\varepsilon} = 1.92$, and $C_\mu = 0.09$.

#### *2.2.1 Modeling the Performance of SCPP*

The Collector

The heat gain of air is given by the following equation:

$$Q = \eta col\ AcolG \tag{8}$$

where, $\eta col,\ Acol$ and $Q$ are the solar collector efficiency, the solar collector and the generated heat due to the effect of the greenhouse.

Q is given by:

$$Q = CN \cdot m\Delta T \tag{9}$$

with,

$$m = \rho air VchAch \tag{10}$$

and,

$$\eta col = \rho air \cdot VchAchCN\Delta T/AcolG \tag{11}$$

where, $Ach,\ Vch$ and $m$ are the surface, the velocity and the mass flow at the entrance to the chimney, respectively.

The Chimney

The chimney efficiency is expressed as:

$$\eta ch = gHch/CNTa \tag{12}$$

where, $Ta$ and $H_{chx}$ are the ambient air temperature and the height of the chimney, respectively.

The total Power is given by:

$$Ntot = \eta_{ch}Q = g(A_{ch}/Ta)\rho colV_{ch}\Delta TAch \tag{13}$$

The pressure difference between the chimney base and the outlet is calculated as follows:

$$\Delta N_{tot} = \rho_{col}gH_{ch}(\Delta T/Ta) \tag{14}$$

#### *2.2.2 The Turbine Model*

Located at the bottom, the wind turbine converts the kinetic energy of the airflow into mechanical rotational energy [22]. The mechanical power drawn in by the turbine is calculated as follows [21]:

$$P_m = \frac{2}{3}\eta_{col}\eta_{ch}A_{col}G \tag{15}$$

The equation above can be further detailed as:

$$P_m = \frac{2}{3}\eta_{col}\eta_{ch}\pi r^2 G \tag{16}$$

$\eta t$ in the present paper is taken to be 0.8 [21,39].

### *2.3 Modeling and Meshing*

The numerical methodology for this study was implemented using Manzanares' SCPP 3D axisymmetric CFD model, which was simulated with ANSYS Fluent software. Because of symmetries along

the YZ and XZ planes, the modeling required only 15° of the pilot plant to accelerate convergence [40]. Because of the irregular shape, triangular meshing is recommended for CFD calculations, as depicted in Fig. 2.

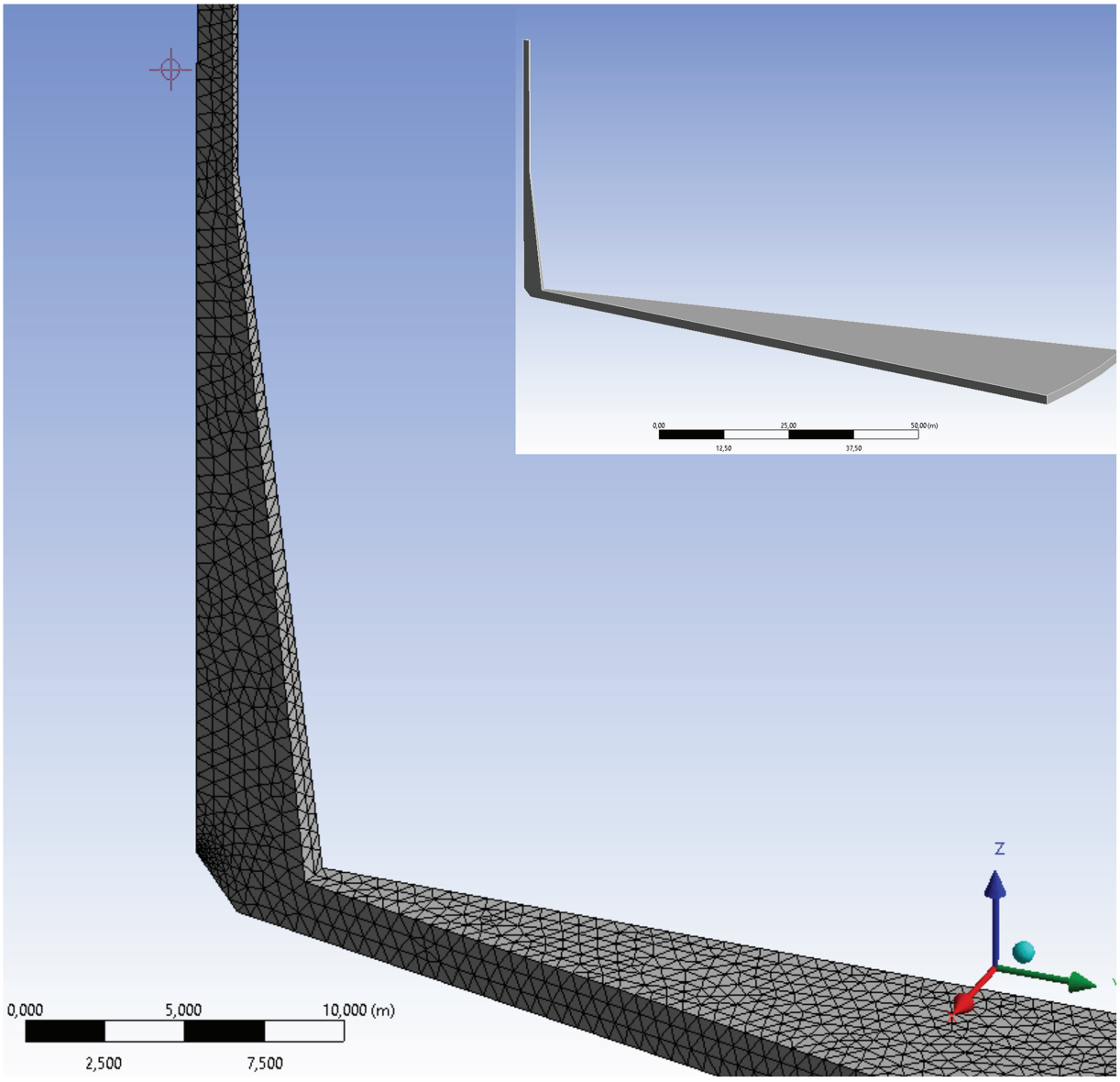


**Figure 2:** Modeling and meshing adopted in CFD analyses

To obtain a mesh-independent answer, various cell count-based computations were performed. Table 1 shows the three mesh configurations used for air temperature (Tm) and air velocity ($Vm$) at the proposed turbine levels. When the number of cells was 299,682, corresponding to 0.4 element dimension, the perceived percentage variation in air velocity ($Vm$) was 0.84%.

This element dimension was used for the entire CFD parametric investigation because it was deemed adequate in comparison to similar efforts in the literature [21].

**Table 1:** Mesh-independent solution results for the CFD analyses

| Elements dimension (m) | Cell counts | Temperature (Tm) K | Change in (Tm) % | Air velocity (Vm) | Change in (Vm) % | Difference from experimental data in (Vm) % |
|---|---|---|---|---|---|---|
| **0.6** | 110,435 | 318.00 | – | 14.69 | – | 1.69 |
| **0.5** | 175,683 | 317.20 | 0.25 | 15.47 | 5.3 | 0.47 |
| **0.4** | 299,682 | 317.00 | 0.06 | 15.60 | 0.84 | 0.60 |

### *2.4 Boundary Conditions*

The appropriate material ties for the ground, chimney, and collector glass as shown in Table 2. The choice of an appropriate turbulence model for describing the physics of the flow field is critical to CFD prediction [41]. The air temperature (T°) is set at 293.15 K. The inlet condition for pressure is designated at the entrance of the domain, whereas a pressure outlet condition is implemented at the exit.

**Table 2:** Material properties

| Physical characteristics | Chimney | Glass | Ground |
|---|---|---|---|
| **Thickness (m)** | 0.0125 | 0.004 | 0.5 |
| **Density (kg/m$^3$)** | 2719 | 2500 | 2160 |
| **Thermal conductivity (W/mK)** | 202.4 | 1.15 | 1.83 |
| **Specific heat (J/kg K)** | 871 | 750 | 710 |
| **Absorption coefficient** | 0 | 0.03 | 0.9 |
| **Transmissivity** | – | 0.9 | – |

The momentum equation was addressed utilizing the RNG k-$\varepsilon$ turbulence model. The correlation between air velocity and pressure was established through a straightforward method. The PRESTO technique was used for the interpolation of pressure. The major equations were approximated with a second-order upwind approach. To solve the radiation equation, we used the discrete ordinates (DO) non-grey radiation approach combined with the solar ray tracing method. The Boussinesq approximation was used to suggest a link between temperature and variations in air density. Using convergence criteria of $10^{-6}$ resulted in optimal simulation accuracy.

### *2.5 Model Validation*

Validation of numerical model results is critical to ensuring their applicability. For this purpose, we applied the numerical model used in this study to the Manzanares pilot plant while maintaining the same material properties (Table 2).

The numerical and experimental data found in the literature [14,21] were compared with the numerical air velocity and air temperature results derived from solar radiations (600, 800, and 1000 W/m$^2$) to verify the accuracy of the current CFD model. Fig. 3 shows air velocity and total temperature contours that are consistent with previous studies, as well as experimental results from the Manzanares Plant. In the following section of the study, the model will be used to investigate the system's performance.

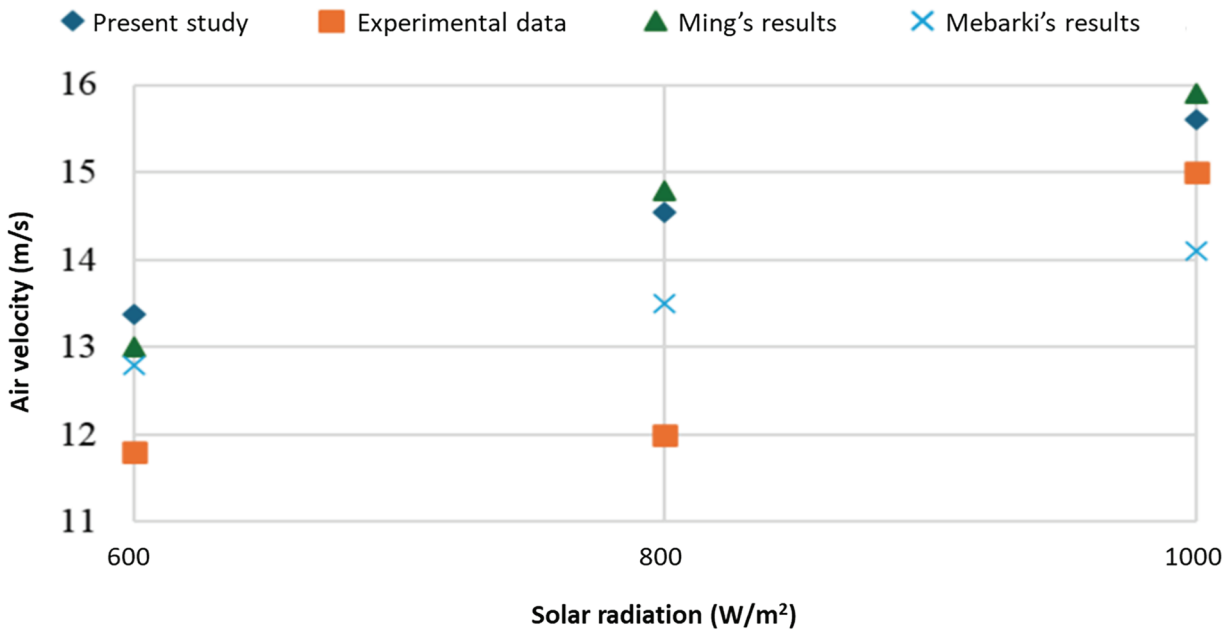


**Figure 3:** Verification of the accuracy of the CFD model by comparing it with certain numerical and experimental data from the literature

## 3 Results and Discussion

Following the application of the CFD model to parametric studies, the following results were obtained.

### *3.1 Air Behavior inside the Chimney*

To better understand the behavior of air movement inside the chimney, and because the results are similar depending on solar radiation, we used the case of 1000 W/m$^2$ solar radiation for each collector radius. Figs. 4 and 5 show the results of the air velocity and pressure simulations within the chimney, respectively. The air velocity increases with variable acceleration along the height of the inverted cone, influenced by the change in pressure difference, reaching its maximum value at the beginning of the cylindrical part at a height of 34 m. As shown in Fig. 6, the air velocity reaches its maximum of 6.89, 10.05, 11.79, 13.23, and 13.75 m/s with collector radius 40, 80, 120, 160, and 200 m, respectively, with pressure differences 22.3, 46.0, 65.0, 79.55, and 90.2 Pa (Fig. 7). The Venturi effect has the shape of the change in velocity explained by the Bernoulli theory and equation of fluid motion (Eq. (17)) [42]:

$$e_t = P + \frac{1}{2}\rho V^2 + \rho g Z = const \tag{17}$$

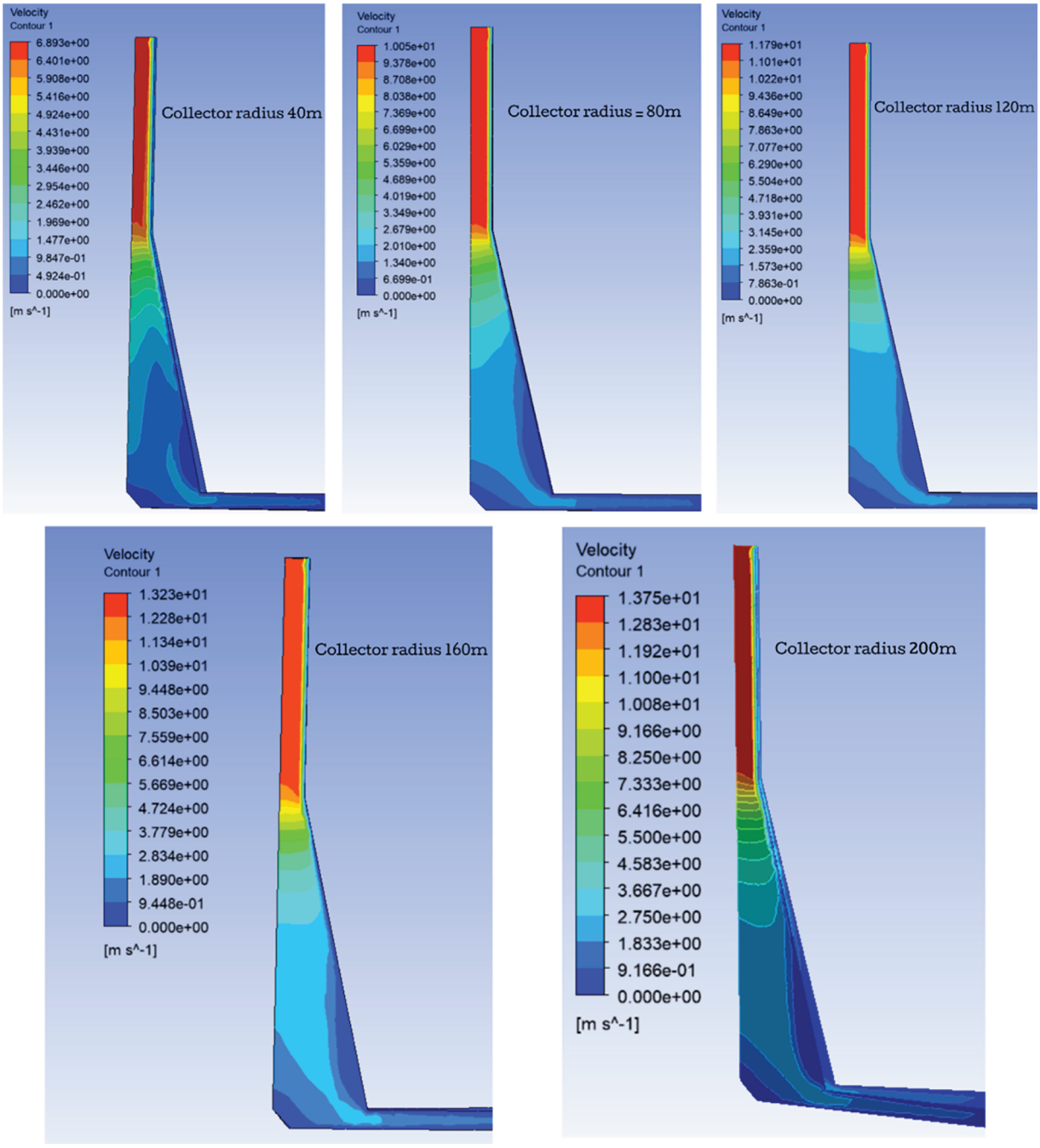


**Figure 4:** The results of the air velocity simulation for five collector radii

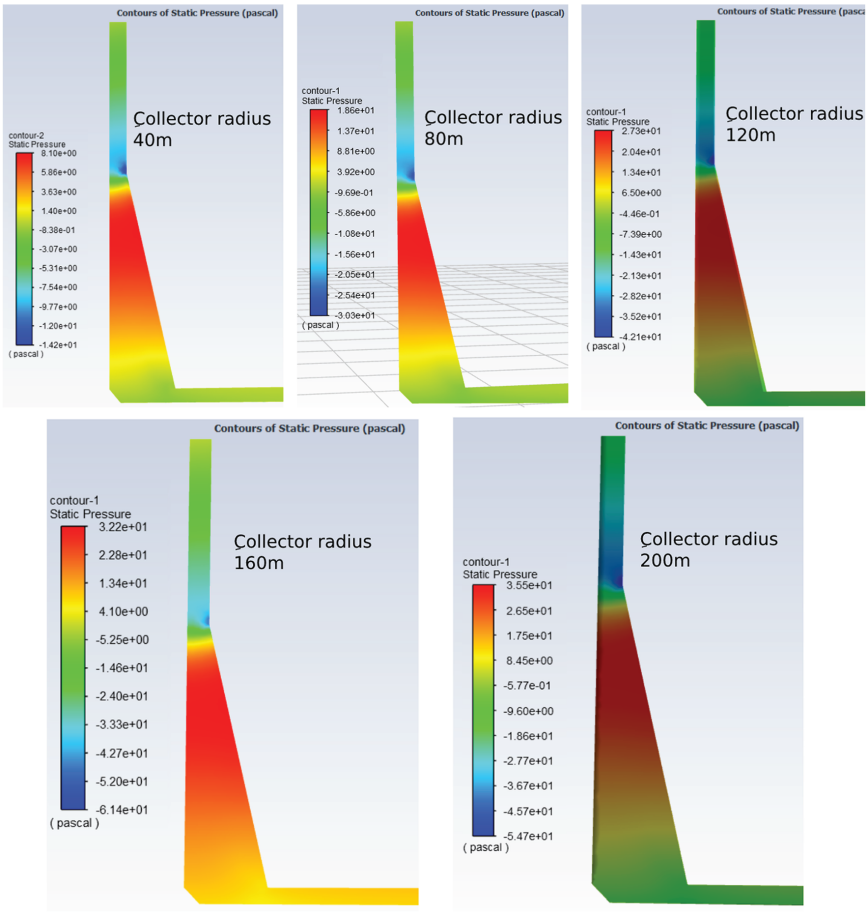


**Figure 5:** The results of the air pressure simulation for five collector radii

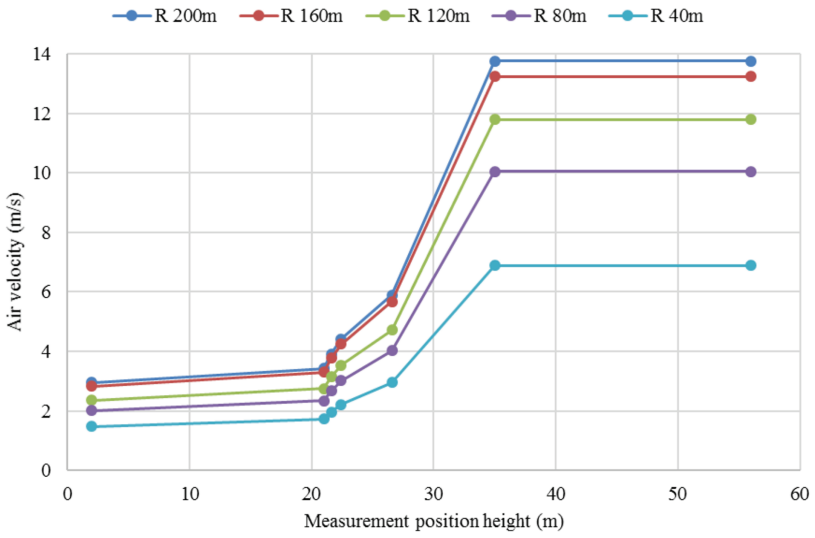


**Figure 6:** Air velocity as a function of measurement location in the chimney for five collector radii

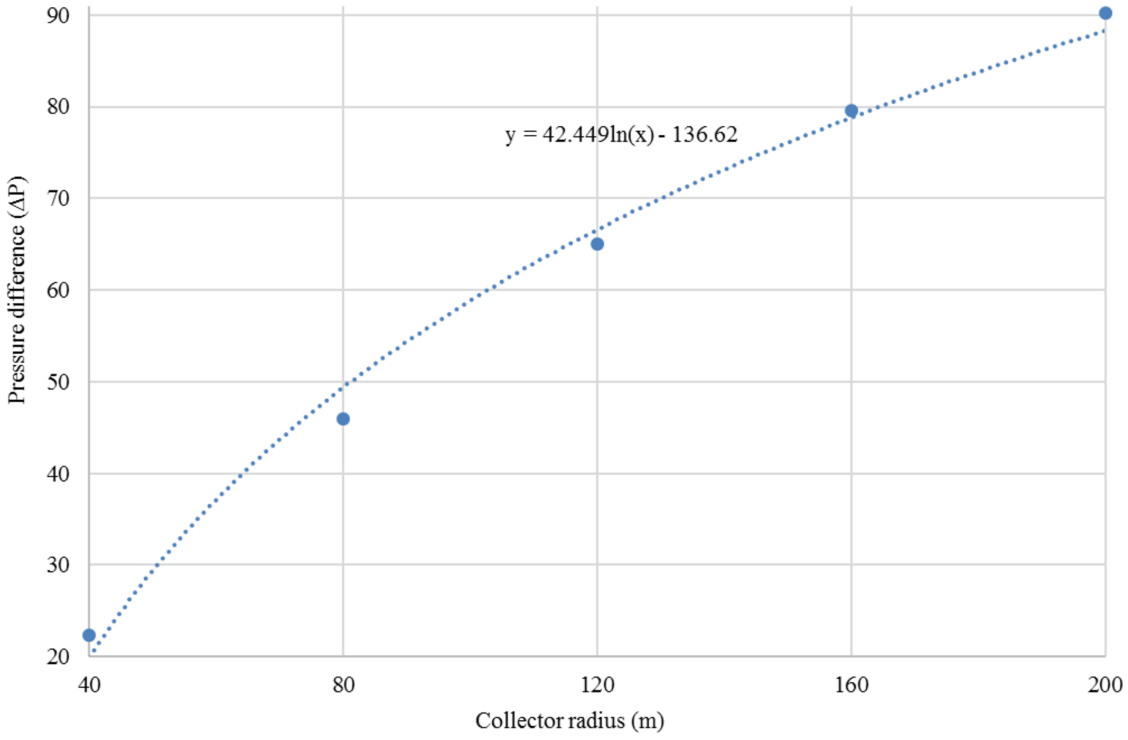


**Figure 7:** The pressure difference for five collector radii

### *3.2 Choosing Turbine Location*

Choosing the best location for the turbine to ensure the system's best energy performance is determined by a number of factors, including the air velocity value and the chimney's cross-sectional area, which are determined by the equation that converts kinetic energy into electrical energy within the chimney. Fig. 8 illustrates how the product of air velocity and the chimney's cross-sectional area varies with changes in measurement height for different collector radii. Fig. 8 shows three intervals, with the best being ≤20 m, followed by 22.4–24.4 and finally ≥34 m. It is worth noting that for the first two intervals, the lowest possible position should be chosen.

Several studies have looked at the minimum air velocity required for a vertical axis turbine to operate efficiently [43,44]. Indeed, the startup wind speed required for power production in vertical axis wind turbines (VAWTs) can be as low as 1 m/s, with some models operating efficiently at 2 m/s [45]. As a result, using the minimum solar radiation proposed in this study as a reference, 400 W/m$^2$, Fig. 9 depicts the proposed model's air velocity curves as a function of collector radius change for five turbine locations. The turbine locations were chosen based on the height intervals mentioned above, which are 2, 20, 22.4, 24.4, and 34 m, respectively. The minimum air velocity threshold line was set at 2 m/s.

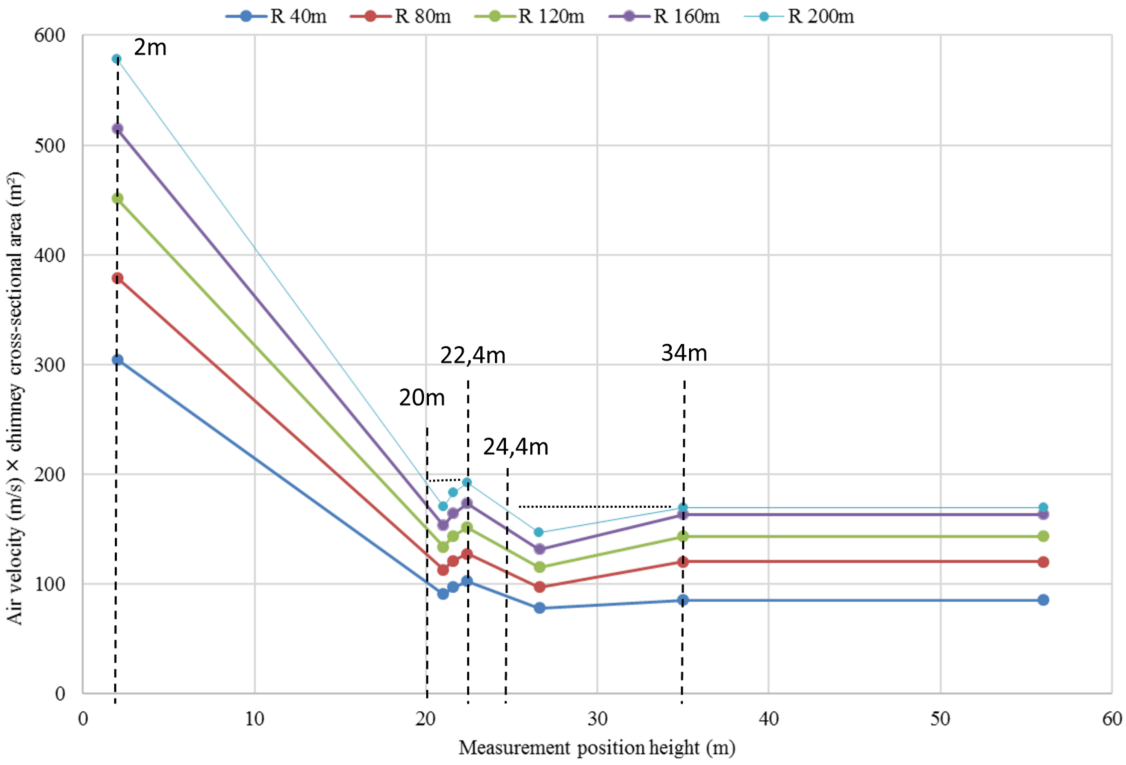


**Figure 8:** The multiplication product of air velocity and chimney cross-section as a function of the change in measuring height for different collector radii

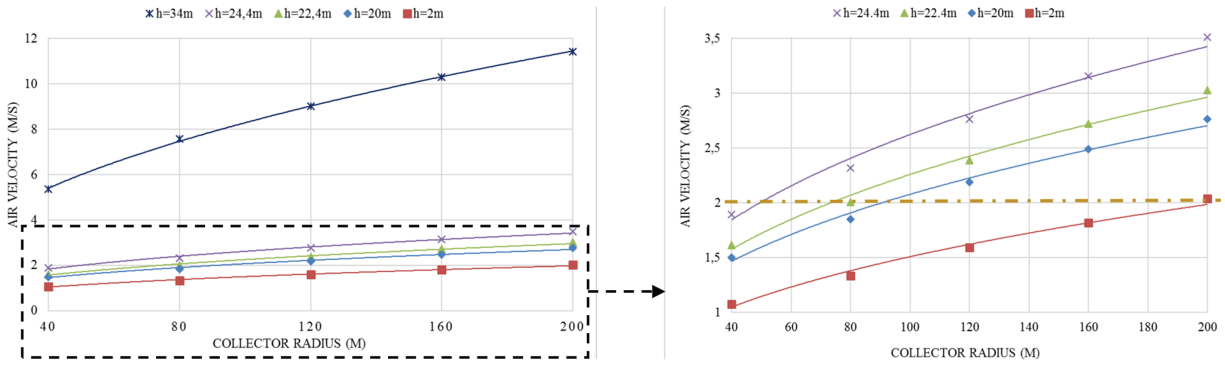


**Figure 9:** The air velocity of the proposed model considering the change in the collector radius, G = 400 W/m$^2$

Based on these findings, it can be noted that the turbine position is determined by five collector radius intervals: 40–50, which corresponds to the turbine position of 34 m; 50–75, which corresponds to the turbine positions of 24.4 and 34 m. Despite the fact that both positions result in the same expected energy, the turbine position 34 m is preferred to reduce turbine costs. The third collector radius interval is 75–90, which corresponds to the turbine position (22.4 m). The next interval is 90–200, which corresponds to a turbine position of 20 m, followed by ≥200, which corresponds to a turbine location of 2 m.

### *3.3 The Produced Electric Energy*

The generated electric energy is calculated using power equations, with the collector radius (r) as the variable. Table 3 provides a guide for using this novel solar chimney model. It displays the generated energy as equations that change depending on the collector radius and solar radiation.

**Table 3:** Equations to calculate the generated energy

| Collector radius ranges (m) | Turbine position (m) | Turbine Radius (m) | Solar radiation W/m$^2$ | | | |
|---|---|---|---|---|---|---|
| | | | 400 | 600 | 800 | 1000 |
| **[40–50]** | 34.0 | 2.25 | $p = 0.0493r^{1.1301}$ | $p = 0.0295r^{1.344}$ | $p = 0.0743r^{1.2094}$ | $p = 0.1504r^{1.1147}$ |
| **[50–75]** | 24.4 | 4.11 | | | | |
| **[75–90]** | 22.4 | 4.5 | $p = 0.0194r^{1.0898}$ | $p = 0.0099r^{1.344}$ | $p = 0.0251r^{1.2089}$ | $p = 0.0507r^{1.1144}$ |
| **[90–200]** | 20.0 | 4.96 | | | | |
| **≥200** | 2 | 9.5 | $p = 0.0154r^{1.1176}$ | $p = 0.009r^{1.3399}$ | $p = 0.0218r^{1.2022}$ | $p = 0.0416r^{1.109}$ |

It also accurately represents the turbine locations and radii for each collector radius interval. In the following section, we will present a practical example of how our model could cover daily electricity needs. Based on the most recent scientific articles that provide a database of electricity consumption in rural dwellings and a large number of rural populations, we chose China, with a rural population of 509,787,562 [46] and India, with a rural population of 893,660,000 (Women and Men in India 2022, 24th Issue) as examples.

According to the literature, the average daily consumption of rural households in India is around 2.150 kW [11], while in China is about 2 kW [47]. Table 4 lists the equations used to calculate the number of electrified houses based on collector radius, solar radiation, and country. As a numerical example, the number of electrified rural houses was calculated using a collector radius of 200 m and solar radiation of 1000 W/m$^2$. The obtained results confirmed that 1 h of solar radiation resulted in the electrification for 24 h of 6.877 rural houses in India or 7.411 rural houses in China.

**Table 4:** Equations to calculate the number of electrified rural houses

| Collector radius ranges (m) | Covered houses (N) | | | | | | | |
|---|---|---|---|---|---|---|---|---|
| | China | | | | India | | | |
| | 400 W/m$^2$ | 600 W/m$^2$ | 800 W/m$^2$ | 1000 W/m$^2$ | 400 W/m$^2$ | 600 W/m$^2$ | 800 W/m$^2$ | 1000 W/m$^2$ |
| **[40–75]** | $0.02465r^{1.1301}$ | $0.0147r^{1.344}$ | $0.0371r^{1.2094}$ | $0.0752r^{1.1147}$ | $0.0229r^{1.1301}$ | $0.0137r^{1.344}$ | $0.0345r^{1.2094}$ | $0.0699r^{1.1147}$ |
| **[75–200]** | $0.0097r^{1.0898}$ | $0.0049r^{1.344}$ | $0.0125r^{1.2089}$ | $0.0253r^{1.1144}$ | $0.009r^{1.0898}$ | $0.0046r^{1.344}$ | $0.0116r^{1.2089}$ | $0.0235r^{1.1144}$ |
| **≥200** | $0.0077r^{1.1176}$ | $0.0045r^{1.3399}$ | $0.0109r^{1.2022}$ | $0.0208r^{1.109}$ | $0.0071r^{1.1176}$ | $0.0041r^{1.3399}$ | $0.0101r^{1.2022}$ | $0.0193r^{1.109}$ |

## 4 Conclusion

This study proposed integrating the solar chimney power plant system with one of the most common types of electricity pylons. The numerical methodology was carried out using Manzanares' SCPP 3D axisymmetric CFD model, which was simulated with ANSYS Fluent software. The RNG k-$\varepsilon$ turbulence model and a discrete ordinates non-grey radiation model were used. The behavior of air inside the chimney was investigated in the first stage. This study determined the optimal turbine positions based on collector radius intervals of 40–50, 50–75, 75–90, 90–200, and ≥200.

Finally, the energy outputs for solar radiation 400, 600, 800, and 1000 W/m$^2$ are presented in the form of equations, with the collector radius as the variable, highlighting the number of rural houses that could be supplied with energy. Our findings confirmed the proposed model's efficiency in generating electricity; for instance, one hour of solar radiation could power 6.877 rural houses in India and 7.411 rural houses in China for 24 h. This study proposes an initiative for electricity transmission companies to invest in infrastructure to supply rural electricity.

**Acknowledgement:** This work was supported by the DGRSDT of the Algerian Ministry of Higher Education and Scientific Research.

**Funding Statement:** The authors received no specific funding for this study.

**Author Contributions:** Ammar Mebarki: Conceptualization, Methodology, Software, Data curation, Writing—original draft preparation, Visualization, Supervision, Writing—reviewing and Editing. Meriem Hafidha Titi: Data curation, Visualization, Software. All authors reviewed the results and approved the final version of the manuscript.

**Availability of Data and Materials:** Not applicable.

**Ethics Approval:** Not applicable.

**Conflicts of Interest:** The authors declare no conflicts of interest to report regarding the present study.

## References

1. Ciancio V, Salata F, Falasca S, Curci G, Golasi I, De Wilde P. Energy demands of buildings in the framework of climate change: an investigation across Europe. Sustain Cities Soc. 2020;60(2007):102213. doi:10.1016/j.scs.2020.102213.
2. Mohammed A, Khan A, Khan HS, Santamouris M. On the cooling energy impacts of combined urban heat mitigation strategies in subtropical urban building environment. Energy Build. 2024;309(12):113918. doi:10.1016/j.enbuild.2024.113918.
3. International Energy Agency. Electricity market report 2023. Paris, France: OECD Publishing; 2023.
4. Shackleton CM, De Vos A. How many people globally actually use non-timber forest products? For Policy Econ. 2022;135(5):102659. doi:10.1016/j.forpol.2021.102659.
5. Uski S, Forssén K, Shemeikka J. Sensitivity assessment of microgrid investment options to guarantee reliability of power supply in rural networks as an alternative to underground cabling. Energies. 2018;11(10):2831. doi:10.3390/en11102831.
6. Gunasekaran M. Polymer concrete insulation technology as a feasible development incubator for rural electric cooperatives & their local communities. In: 2020 IEEE Electrical Insulation Conference (EIC); 2020 Jun 22–Jul 3; Knoxville, TN, USA. p. 154–6. doi:10.1109/eic47619.2020.9158686.
7. Alstone P, Gershenson D, Kammen DM. Decentralized energy systems for clean electricity access. Nature Clim Change. 2015;5(4):305–14. doi:10.1038/nclimate2512.
8. Yang Y, Si Z, Jia L, Wang P, Huang L, Zhang Y, et al. Whether rural rooftop photovoltaics can effectively fight the power consumption conflicts at the regional scale-a case study of Jiangsu Province. Energy Build. 2024;306:113921. doi:10.1016/j.enbuild.2024.113921.
9. Urpelainen J. Energy poverty and perceptions of solar power in marginalized communities: survey evidence from Uttar Pradesh. India Renew Energy. 2016;85(1):534–9. doi:10.1016/j.renene.2015.07.001.

10. Kale SS. Current reforms: the politics of policy change in India's electricity sector. Pac Aff. 2004;77(3): 467–91.
11. Conevska A, Urpelainen J. Weathering electricity demand? Seasonal variation in electricity consumption among off-grid households in rural India. Energy Res Soc Sci. 2020;65(4):101444. doi:10.1016/j.erss.2020.101444.
12. Martinot E, Chaurey A, Lew D, Moreira JR, Wamukonya N. Renewable energy markets in developing countries. Annu Rev Energy Environ. 2002;27(1):309–48. doi:10.1146/annurev.energy.27.122001.083444.
13. Aklin M, Bayer P, Harish SP, Urpelainen J. Information and energy policy preferences: a survey experiment on public opinion about electricity pricing reform in rural India. Econ Gov. 2014;15(4):305–27. doi:10.1007/s10101-014-0146-5.
14. Abo-Zahhad EM, Hachicha AA, Mistarihi MZ, Salim MH, Esmail MFC. Optimization of ground material properties for enhanced solar chimney power plant efficiency: a CFD and RSM approach. Energy Rep. 2025;13(4):3929–45. doi:10.1016/j.egyr.2025.03.035.
15. Elsayed I, Nishi Y. A feasibility study on power generation from solar thermal wind tower: inclusive impact assessment concerning environmental and economic costs. Energies. 2018;11(11):3181. doi:10.3390/en11113181.
16. Maghrebi MJ, Masoudi Nejad R. Performance evaluation of floating solar chimney power plant in Iran: estimation of technology progression and cost investigation. IET Renew Power Gener. 2017;11(13):1659–66. doi:10.1049/iet-rpg.2016.0963.
17. Kumar Mandal D, Biswas N, Manna NK, Benim AC. Impact of chimney divergence and sloped absorber on energy efficacy of a solar chimney power plant (SCPP). Ain Shams Eng J. 2024;15(2):102390. doi:10.1016/j.asej.2023.102390.
18. Khaleel OJ, Basim Ismail F, Khalil Ibrahim T, bin Abu Hassan SH. Energy and exergy analysis of the steam power plants: a comprehensive review on the classification, development, improvements, and configurations. Ain Shams Eng J. 2022;13(3):101640. doi:10.1016/j.asej.2021.11.009.
19. Hurtado FJ, Kaiser AS, Zamora B. Evaluation of the influence of soil thermal inertia on the performance of a solar chimney power plant. Energy. 2012;47(1):213–24. doi:10.1016/j.energy.2012.09.040.
20. Das P, Chandramohan VP. 3D numerical study on estimating flow and performance parameters of solar updraft tower (SUT) plant: impact of divergent angle of chimney, ambient temperature, solar flux and turbine efficiency. J Clean Prod. 2020;256(12):120353. doi:10.1016/j.jclepro.2020.120353.
21. Cuce E, Sen H, Cuce PM. Numerical performance modelling of solar chimney power plants: influence of chimney height for a pilot plant in Manzanares. Spain Sustain Energy Technol Assess. 2020;39(1):100704. doi:10.1016/j.seta.2020.100704.
22. Schlaich J. The solar chimney: electricity from the sun. Fellbach, Germany: Edition Axel Menges; 1995.
23. Titi MH, Mebarki A, Assassi A. Integration of the Manzanares solar chimney power plants in towers: collector and building height configuration. Eng Technol Appl Sci Res. 2025;15(3):23002–7. doi:10.48084/etasr.10594.
24. Wang B, Adolphe L, Cot LD. New building typology for solar chimney electricity. In: New urban configurations. Amsterdam, The Netherlands: IOS Press; 2014. p. 293–8. doi:10.3233/978-1-61499-365-0-298.
25. National Grid Group. Facts about electricity pylons [Online]. [cited 2024 Oct 21]. Available from: https://www.nationalgrid.com/stories/energy-explained/everything-you-ever-wanted-know-about-electricity-pylons.
26. Avoiding Danger from Overhead Power Lines [Online]. [cited 2024 Oct 21]. Available from: https://www.hse.gov.uk/pubns/gs6.htm.
27. Lookout. Lookup: the use of mechanical plant in the vicinity of electricity overhead lines [Online]. [cited 2024 Oct 21]. Available from: https://www.energynetworks.org/assets/images/Resource%20library/LookoutLookup_070918%20The%20Use%20of%20Mechanical%20Plant%20%20DUE%20REVIEW.pdf?1717178275.

28. Perales J, Zapata G, Raymundo C. Energy model based on fluvial rainfall for the rural population with torrential rain. In: Proceedings of the 4th Brazilian Technology Symposium (BTSym'18). Cham, Switzerland: Springer International Publishing; 2019. p. 171–9. doi:10.1007/978-3-030-16053-1_16.
29. Mebarki A, Sekhri A, Assassi A, Hanafi A, Marir B. CFD analysis of solar chimney power plant: finding a relationship between model minimization and its performance for use in urban areas. Energy Rep. 2022;8(5):500–13. doi:10.1016/j.egyr.2021.12.008.
30. Ayadi A, Nasraoui H, Bouabidi A, Driss Z, Bsisa M, Abid MS. Effect of the turbulence model on the simulation of the air flow in a solar chimney. Int J Therm Sci. 2018;130:423–34. doi:10.1016/j.ijthermalsci.2018.04.038.
31. Yoo S, Oh S, Hachicha AA. Numerical simulation and performance evaluation of filter-equipped solar chimney power plants. Appl Therm Eng. 2023;218(3):119284. doi:10.1016/j.applthermaleng.2022.119284.
32. Elwekeel FNM, Abdala AMM, Rahman MM. Effects of novel collector roof on solar chimney power plant performance. J Sol Energy Eng. 2019;141(3):031004. doi:10.1115/1.4041403.
33. Bouabidi A, Ayadi A, Nasraoui H, Driss Z, Abid MS. Study of solar chimney in Tunisia: effect of the chimney configurations on the local flow characteristics. Energy Build. 2018;169(1):27–38. doi:10.1016/j.enbuild.2018.01.049.
34. Nasraoui H, Driss Z, Kchaou H. Novel collector design for enhancing the performance of solar chimney power plant. Renew Energy. 2020;145(4):1658–71. doi:10.1016/j.renene.2019.07.062.
35. Asnaghi A, Ladjevardi SM. Solar chimney power plant performance in Iran. Renew Sustain Energy Rev. 2012;16(5):3383–90. doi:10.1016/j.rser.2012.02.017.
36. Gholamalizadeh E, Chung J. A comparative study of CFD models of a real wind turbine in solar chimney power plants. Energies. 2017;10(10):1674. doi:10.3390/en10101674.
37. ANSYS FLUENT User's Guide 13.0 [Online]. [cited 2024 Oct 21]. Available from: https://www.afs.enea.it/project/neptunius/docs/fluent/html/ug/node464.htm.
38. Gholamalizadeh E, Kim MH. Three-dimensional CFD analysis for simulating the greenhouse effect in solar chimney power plants using a two-band radiation model. Renew Energy. 2014;63(1):498–506. doi:10.1016/j.renene.2013.10.011.
39. Nizetic S, Ninic N, Klarin B. Analysis and feasibility of implementing solar chimney power plants in the Mediterranean region. Energy. 2008;33(11):1680–90. doi:10.1016/j.energy.2008.05.012.
40. Biswas N, Kumar Mandal D, Manna NK, Cemal Benim A. Novel stair-shaped ground absorber for performance enhancement of solar chimney power plant. Appl Therm Eng. 2023;227(1):120466. doi:10.1016/j.applthermaleng.2023.120466.
41. Liu J, Niu J. CFD simulation of the wind environment around an isolated high-rise building: an evaluation of SRANS, LES and DES models. Build Environ. 2016;96:91–106. doi:10.1016/j.buildenv.2015.11.007.
42. Gilbert-Kawai ET, Wittenberg MD. Bernoulli equation and venturi effect. In: Essential equations for anaesthesia: key clinical concepts for the FRCA and EDA. Cambridge, UK: Cambridge University Press; 2014. p. 26–7.
43. Ali M, Gherissi A, Altaharwah Y. Experimental and simulation study on a rooftop vertical-axis wind turbine. Open Eng. 2023;13(1):20220465. doi:10.1515/eng-2022-0465.
44. Aravind Vaithilingam C, Sivasubramanian R, Prakash OKS, Misron N, Happonen A. Triple rotor vertical axis wind turbine for low wind speed range energy generation. E3S Web Conf. 2024;488:02009. doi:10.1051/e3sconf/202448802009.
45. Francis MF, Ajayi OO, Ojo JO. Development of a novel airfoil for low wind speed vertical axis wind turbine using QBlade simulation tool. Fuel Commun. 2021;9(1):100028. doi:10.1016/j.jfueco.2021.100028.
46. Communiqué of the Seventh National Population Census (No. 7) [Online]. [cited 2024 Oct 21]. Available from: https://www.stats.gov.cn/english/PressRelease/202105/t20210510_1817192.html.

47. Nie Y, Zhang G, Zhong L, Su B, Xi X. Urban—rural disparities in household energy and electricity consumption under the influence of electricity price reform policies. Energy Policy. 2024;184(1):113868. doi:10.1016/j.enpol.2023.113868.